Article

Unraveling Solvent-Driven Equilibria between □- and 3-Helices through an Integrated Spin Labeling and Computational Approach

Silvia Carlotto, Paola Cimino, Mirco Zerbetto, Lorenzo Franco, Carlo Corvaja, Marco Crisma, Fernando Formaggio, Claudio Toniolo, Antonino Polimeno, and Vincenzo Barone

J. Am. Chem. Soc., **2007**, 129 (36), 11248-11258• DOI: 10.1021/ja073516s • Publication Date (Web): 18 August 2007

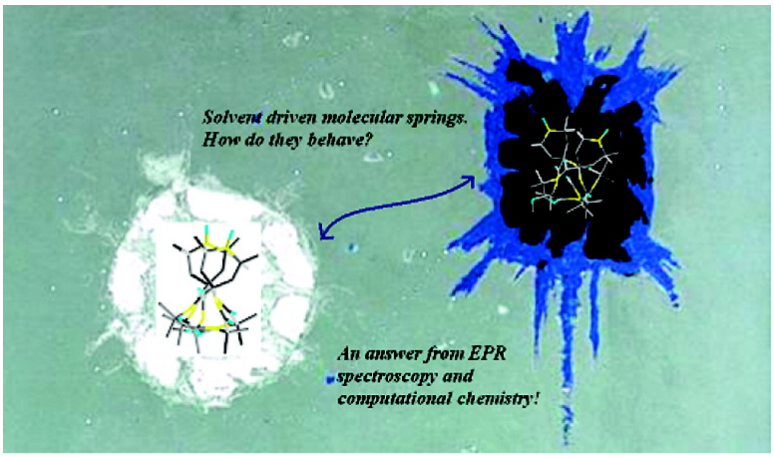

J|A|C|S
ARTICLES
Published on Web 08/18/2007

Unraveling Solvent-Driven Equilibria between α- and 3_{10}-Helices through an Integrated Spin Labeling and Computational Approach

Silvia Carlotto,[†] Paola Cimino,[§,||] Mirco Zerbetto,[†] Lorenzo Franco,[†] Carlo Corvaja,[†] Marco Crisma,[‡] Fernando Formaggio,[†,‡] Claudio Toniolo,[†,‡] Antonino Polimeno,*[,†] and Vincenzo Barone*[,§]

Contribution from the Dipartimento di Scienze Chimiche, Università degli Studi di Padova, Via Marzolo 1, I-35131 Padova, Italy, Istituto di Chimica Biomolecolare, CNR, Unità di Padova, Via Marzolo 1, I-35131 Padova, Italy, Dipartimento di Chimica and CR-INSTM Village, Università di Napoli "Federico II", Complesso Universitario di Monte Sant'Angelo, Via Cintia, I-80126 Napoli, Italy, and Dipartimento di Scienze Farmaceutiche, Università di Salerno, via Ponte Don Melillo, 84084 Fisciano-Salerno, Italy

Received May 17, 2007; E-mail: antonino.polimeno@unipd.it; baronev@unina.it

Abstract: In this work we present an effective and flexible computational approach, which is the result of an ongoing development in our groups, allowing the complete *a priori* simulation of the ESR spectra of complex systems in solution. The usefulness and reliability of the method are demonstrated on the very demanding playground represented by the tuning of the equilibrium between 3_{10}- and α-helices of polypeptides by different solvents. The starting point is the good agreement between computed and X-ray diffraction structures for the 3_{10}-helix adopted by the double spin-labelled heptapeptide Fmoc-(Aib-Aib-TOAC)$_2$-Aib-OMe. Next, density functional computations, including dispersion interactions and bulk solvent effects, suggest another energy minimum corresponding to an α-helix in polar solvents, which, eventually, becomes the most stable structure. Computation of magnetic and diffusion tensors provides the basic ingredients for the building of complete spectra by methods rooted in the Stochastic Liouville Equation (SLE). The remarkable agreement between computed and experimental spectra at different temperatures allowed us to identify helical structures in the various solvents. The generality of the computational strategy and its implementation in effective and user-friendly computer codes pave the route toward systematic applications in the field of biomolecules and other complex systems.

1. Introduction

A better understanding of the properties and function of complex systems requires integrated strategies in which well-defined models are investigated by both experimental and theoretical approaches. In the specific field of proteins, it is well recognized that polypeptides represent suitable models for a number of properties, and several experimental techniques have been systematically applied to their study. Unfortunately, interpretation of experimental results is not without ambiguities either because of the role of different environmental effects (e.g., crystal state for X-ray diffraction) or because the relationship between spectroscopic and structural/dynamics characteristics is only indirect. Here, theoretical approaches come into play provided that they are able to couple reliability and feasibility for large systems.

Until quite recently, quantum mechanical (QM) computations of biomolecules were essentially restricted to the structural characteristics of relatively small models in the gas phase. However, the development of powerful methods, integrating the most recent models rooted into the density functional theory (DFT)[1] and discrete-continuum descriptions of solvent effects,[2] is paving the route toward the description of more realistic systems in their natural (aqueous) environment.[3] Direct comparison with experimental results then calls for the concomitant computation of reliable structural and spectroscopic parameters taking dynamical effects into the proper account.[4] Although this is, in general, a quite ambitious long-term target, under some favorable circumstances we can already obtain remarkable results. In the particular case of electron spin resonance (ESR) spectroscopy, we have recently shown that proper use of different time scales can allow the complete *a priori* simulation

[†] Università degli Studi di Padova.
[‡] Istituto di Chimica Biomolecolare CNR, Padova.
[§] Università di Napoli, "Federico II".
[||] Università di Salerno.

(1) Koch, W.; Holthousen, W. C. *A Chemist's Guide to Density Functional Theory*; Wiley-VCH: Weinheim, 2000.
(2) Tomasi, J.; Mennucci, B.; Cammi, R. *Chem. Rev.* **2005**, *105*, 2999.
(3) (a) Brancato, G.; Rega, N.; Barone, V. *J. Chem. Phys.* **2006**, *125*, 164515. (b) Gustavsson, T.; Banyasz, A.; Lazzarotto, E.; Markovitsi, D.; Scalmani, G.; Frisch, M.; Improta, R.; Barone, V. *J. Am. Chem. Soc.* **2006**, *128*, 607. (c) Improta, R.; Santoro, F.; Barone, V. *Theor. Chem. Acc.* **2007**, *117*, 1073.
(4) (a) Improta, R.; Barone, V.; Santoro, F. *Angew. Chem., Int. Ed.* **2007**, *46*, 405. (b) Santoro, F.; Improta, R.; Lami, A.; Bloino, J.; Barone, V. *J. Chem. Phys.* **2007**, *126*, 084509. (c) Brancato, G.; Rega, N.; Barone, V. *Theor. Chem. Acc.* **2007**, *117*, 1001. (d) Barone, V.; Polimeno, A. *Chem. Soc. Rev.* **2007**, DOI: 10.1039/b515155b.

10.1021/ja073516s CCC: $37.00

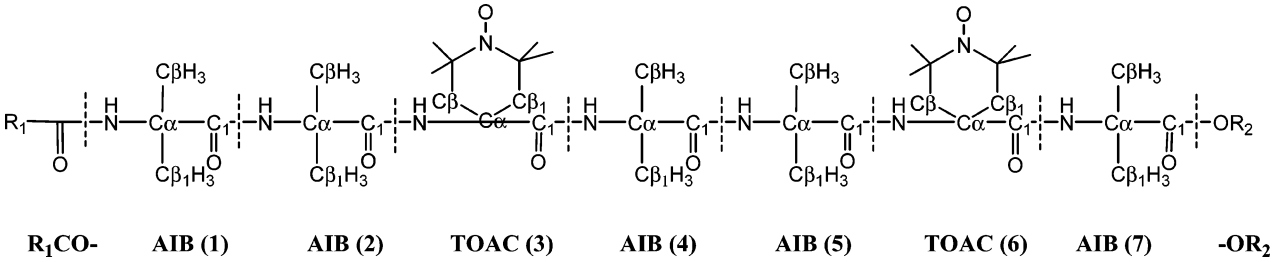

Figure 1. Chemical structure of Fmoc-(Aib-Aib-TOAC)$_2$-Aib-OMe (heptapeptide **1**). R_1 = 9-fluorenylmethoxy and R_2 = Me.

of experimental spectra.[5] In particular, a new general computational approach combining QM calculations of structures and magnetic tensors with the treatment of rotational diffusion in solution by the stochastic Liouville equation (SLE) approach leads to remarkable agreement between experimental and computed spectra for a number of test cases.[6,7] Extension and validation of this approach to labeled biomolecules would then provide access to information of unprecedented richness and reliability by combining experimental and computational methodologies. Since peptides are well recognized models for studying stability and folding of helical regions of proteins, we decided to tackle the complete task of characterizing the solvent-driven equilibrium between different helical forms of a nitroxide doubly labeled peptide by characterizing at the same time its 3D-structure and complete ESR spectrum in different solvents and at different temperatures. It should be pointed out that the ESR spectral features depend not only on the distance between the labels but also on the relative orientations of the principal axes of the electron dipolar interaction tensor, the nitroxide label ***g*** tensor, the ^{14}N hyperfine tensors, and the diffusion tensor. Thus, agreement between experimental spectra and their counterparts issuing from QM structures and magnetic tensors through solution of the SLE represents a convincing demonstration of the correctness of the predicted structure. This approach is particularly interesting when different peptide conformations with slightly diverging energies (like, e.g., 3_{10}- and α-helices) are available and the peptide can predominantly fold in one of them biased by temperature and/or solvent characteristics.

In the past decades, double spin labeling of peptides and proteins by stable nitroxide radicals has provided remarkable information: in particular, continuous wave (CW) and pulse [e.g., double quantum coherence (DQC) and PELDOR] ESR spectra of double spin labeled systems have been studied.[8−10] The sensitivity of DQC and PELDOR[11,12] spectra allows the reliable determination of distances between labels in the range 1.6−6.0 nm in frozen solution, whereas shorter distances are not accessible because the electron dipolar interaction becomes too large and the presence of relevant scalar electron exchange interactions prevents the irradiation of a single electron spin, which is the prerequisite for their application.[13]

On the other hand, when the spin labels are at short distances, the liquid solution CW-ESR spectrum could be very informative because its shape depends on several structural and dynamic parameters which characterize the double labeled peptide.

In this paper we present the results of a CW-ESR investigation of the double spin labeled, terminally protected, heptapeptide Fmoc-(Aib−Aib-TOAC)$_2$-Aib-OMe (**1**) (Fmoc, fluorenyl-9-methoxycarbonyl; Aib, α-aminoisobutyrric acid; TOAC, 2,2,6,6-tetramethylpiperidine-1-oxyl-4-amino, 4-carboxylic acid; OMe, methoxy), which is characterized by the presence of two TOAC nitroxide free radicals at relative positions i, $i + 3$ (Figure 1) in different solvents and at several temperatures. Aib[14−16] and TOAC[17] are two strongly helicogenic, C^{α}-tetrasubstituted, α-amino acids. The CW-ESR spectra have been compared with their theoretical counterparts pertaining to the deepest energy minima obtained by QM computations (3_{10}- and α-helix). It will be shown that in specific solvents the experimental spectra agree well with those expected for the 3_{10}-helix, in other solvents with those predicted for the α-helix, while for a final set of solvents with those associated with a mixture of α- and 3_{10}-helices with temperature-dependent relative percentages.

The α- and 3_{10}-helices are two common polypeptide conformations.[18−21] The former helix is a well-known secondary structural element in proteins. The 3_{10}-helix it not as widespread as the α-helix, but it is still rather frequently found in proteins, especially as a N- or C-terminal extension of an α-helix. The 3_{10}-helices are usually quite short (about four residues in length), although 3_{10}-helices of 7−12 residues[15,19,22,23] in length have been authenticated in proteins. 3_{10}-Helices have been proposed as intermediates in the folding/unfolding processes of α-helices[24] because there is a lower entropic penalty for the onset of the bend required for the formation of the intramolecular $i \leftarrow i +$

(5) Polimeno, A.; Barone, V. *Phys. Chem. Chem. Phys*. **2006**, *8*, 4609.
(6) Barone, V.; Brustolon, M.; Cimino, P.; Polimeno, A.; Zerbetto, M.; Zoleo, A. *J. Am. Chem. Soc.* **2006**, *128*, 15865.
(7) Zerbetto, M.; Carlotto, S.; Polimeno, A.; Corvaja, C.; Franco, L.; Toniolo, C.; Formaggio, F.; Barone, V.; Cimino, P. *J. Phys. Chem. B* **2007**, *111*, 2668.
(8) Hubbell, W. L.; Mchaourab, H. S.; Altenbach, C.; Litzow, M. A. *Structure* **1966**, *4*, 779.
(9) Steinhoff, H. J. *Frontiers in Bioscience* **2002**, *7*, 97.
(10) Eaton, S. S.; Eaton, G. R. In *Biological Magnetic Resonance*; Berliner, L. J., Eaton, S. S., Eaton, G. R., Eds.; Kluwer Academic/Plenum Publishers: New York, 2000; Vol 19, pp 2−28.
(11) Tsvetkov, Yu. D. In *Biological Magnetic Resonance*; Berliner, L. J., Bender, C. J., Eds.; Kluwer Academic/Plenum Publishers: New York, 2004; Vol. 21, pp 385−433.
(12) Jeske, G.; Pannier, M.; Spiess, H. W. In *Biological Magnetic Resonance*; Berliner, L. J., Eaton, S. S., Eaton, G. R., Eds.; Kluwer Academic/Plenum Publishers: New York, 2000; Vol. 19, pp 493−512.
(13) Borbat, P. P.; Freed, J. F. In *Biological Magnetic Resonance*; Berliner, L. J., Eaton, S. S., Eaton, G. R., Eds.; Kluwer Academic/Plenum Publishers: New York, 2000; Vol. 19, pp 383−460.
(14) Karle, I. L.; Balaram, P. *Biochemistry* **1990**, *29*, 6747.
(15) Toniolo, C.; Crisma, M.; Formaggio, F.; Peggion, C. *Biopolymers (Pept. Sci.)* **2001**, *60*, 396.
(16) Improta, R.; Kudin, K. N.; Scuseria, G. E.; Barone, V. *J. Am. Chem. Soc.* **2001**, *123*, 3311.
(17) (a) Toniolo, C.; Crisma, M.; Formaggio, F. *Biopolymers* (*Pept. Sci.*) **1998**, *47*, 153. (b) Crisma, M.; Deschamps, J. R.; George, C.; Flippen-Anderson, J. L.; Kaptein, B.; Broxterman, Q. B.; Moretto, A.; Oancea, S.; Jost, M.; Formaggio, F.; Toniolo, C. *J. Pept. Res.* **2005**, *65*, 564.
(18) Barlow, D. J.; Thornton, J. M. *J. Mol. Biol.* **1988**, *201*, 601.
(19) Toniolo, C.; Benedetti, E. *Trends Biochem. Sci*. **1991**, *16*, 350.
(20) Armen, R.; Alonso, D. O. V.; Daggett, V. *Protein Sci.* **2003**, *12*, 1145.
(21) Bolin, K. A.; Millhauser, G. L. *Acc. Chem. Res*. **1999**, *32*, 1027.
(22) Smythe, M. L.; Huston, S. E.; Marshall, G. R. *J. Am. Chem. Soc.* **1995**, *117*, 5445.
(23) Smythe, M. L.; Nakaie, C. R.; Marshall, G. R. *J. Am. Chem. Soc.* **1995**, *117*, 10555.
(24) Millhauser, G. L. *Biochemistry* **1995**, *34*, 3873.

3 *versus* $i \leftarrow i + 4$ hydrogen bonds. The relative stability in solution of these two ordered secondary structures depends on various factors. The major parameters are the peptide main-chain length, the amino acid sequence, the Aib content, and the solvent dielectric properties.[15,19,22,23,25−27] Relatively short oligopeptides rich in Aib have been observed to largely prefer 3_{10}-helical structures in nonaqueous solutions.[16,19,28] It has been also suggested that the asymmetric geometry adopted by the Aib residue can favor the 3_{10}- over the α-helix.[29]

This paper is organized as follows. In section 2 we summarize the experimental procedures followed by the spectroscopic characterization (via CW-ESR) of heptapeptide **1**. Modeling is treated in section 3. A detailed discussion of the results of the simulations and general conclusions are outlined in sections 4 and 5, respectively.

2. Experimental Section

Synthesis. The solution synthesis and analytical characterization of heptapeptide **1** are described in ref 7.

X-ray Diffraction. Single crystals of Fmoc-(Aib-Aib-TOAC)$_2$-Aib-OMe (heptapeptide **1**) were grown by slow evaporation from a TFE (2,2,2-trifluoroethanol) solution. The asymmetric unit is composed of one peptide molecule and two cocrystallized TFE molecules. Formula $C_{60}H_{89}F_6N_9O_{14}$, $M = 1274.40$, monoclinic, space group $P2_1/c$, unit cell dimensions $a = 18.813(3)$ Å, $b = 17.134(3)$ Å, $c = 22.355(4)$ Å, $\beta = 104.37(7)°$; $V = 6981(2)$ Å^3, $Z = 4$; $d_{calcd} = 1.213$ g cm^{-3}. Crystal size and color: $0.40 \times 0.20 \times 0.05$ mm^3, orange. Absorption coefficient (Cu Kα) = 0.817 mm^{-1}. Intensity data were collected at room temperature with Cu Kα radiation ($\lambda = 1.541\,78$ Å) using a Philips PW 1100 diffractometer in the $\theta-2\theta$ scan mode up to $\theta = 54.2°$ (0.95 Å resolution). The crystal did not significantly diffract at higher resolution. The structure was solved by direct methods with the SIR 2002 program.[30] Refinement was carried out by least-squares procedures on F^2, using all data, by application of the SHELXL 97 program.[31] All non-hydrogen atoms were refined anisotropically. Restraints were applied to the anisotropic displacement parameters of the atoms of the two cocrystallized solvent molecules. Hydrogen atoms were calculated at idealized positions and refined using a riding model. The final R indices were $R_1 = 0.0890$, $wR_2 = 0.2241$ [$I > 2\sigma(I)$] and $R_1 = 0.1142$, $wR_2 = 0.2672$ (all data). Data/restraints/parameters: 8491/72/779. Goodness of fit on F^2: 1.140. The largest peak and hole in the final difference Fourier map were 0.81 and −0.41 e Å^{-3}, respectively. Crystallographic data (including atomic coordinates, bond distances, bond angles, torsion angles, intra- and intermolecular H-bonds parameters) may be found in the Supporting Information as a CIF file.

ESR Characterization. The ESR spectra were recorded using an X-band (9.5 GHz) Bruker ER200D spectrometer. Temperature control was achieved using a Bruker BVT2000 nitrogen-flow system. For the ESR measurements a 10^{-4} M solution of the heptapeptide **1** in MeCN was prepared and put into quartz tubes of 1 mm inner diameter. The solution in the tubes was carefully degassed in a *vacuum* line by several pump−freeze−thaw cycles and finally sealed off.

The high-temperature (330 K) ESR spectrum of heptapeptide **1** in MeCN consists of five lines deriving from the hyperfine coupling of the unpaired electrons with two ^{14}N nuclei, as expected for a double nitroxide system with an exchange interaction larger than the ^{14}N hyperfine coupling. The relative peak-to-peak intensities of the hyperfine components deviate from the 1:2:3:2:1 ratios, corresponding to the degeneracy of the transitions for a two $I = 1$ nuclear spins system. In particular, the heights of the second and fourth lines are lower. By lowering the temperature, the overall spectrum broadens and the variation in heights becomes more pronounced. A similar behavior was observed in the remaining solvents considered in this work, i.e., methanol, toluene, and chloroform.

3. Modeling

From the CW-ESR spectra it is possible to obtain both dynamic and structural information. In the case of fast motion of the labeled molecules the structural information can be derived from a fast-motional perturbative model. On the other hand, in the slow motion regime a more sophisticated theoretical approach is required, due to the profound effects that molecular motions exert on the spin relaxation processes. ESR spectroscopy in the slow-motion regime can be interpreted effectively within the SLE. A new integrated approach to the *ab initio* modeling of CW-ESR presented elsewhere[5] is composed of several ingredients: (i) state-of-the-art QM calculations providing the structural and local magnetic properties of the molecular system under investigation, (ii) calculation of dissipative parameters, such as rotational diffusion tensors, using standard hydrodynamic arguments, and, (iii) in the case of multiply labeled systems, computation of the electron exchange and dipolar interactions. Let us point out in this connection that in conventional spectra simulation the two steps of guessing the magnetic parameters and of simulating the spectral profile are completely disentangled. On the contrary, our approach requires self-consistency between magnetic and diffusive parameters, which are both related to the geometrical structure issuing from *a priori* geometry optimization or short-time dynamics.

Simulation of the ESR spectra is based on the implementation of the SLE introduced by Freed and co-workers.[32,33] In the standard approach the SLE

$$\frac{\partial \rho(Q,t)}{\partial t} = -i[\hat{H}(Q),\rho(Q,t)] - \hat{\Gamma}(Q)\,\rho(Q,t) \qquad (1)$$

describes the time evolution of the density matrix of the system, depending upon general stochastic coordinates Q, and controlled by the stochastic operator $\hat{\Gamma}$. The equation is defined with respect to $\hat{H}$,[5] the magnetic Hamiltonian of the system which includes Zeeman, hyperfine, exchange, and dipolar interactions for the two TOAC residues:

$$\hat{H} = \frac{\beta_e}{\hbar}\sum_i \vec{B}_0 \cdot \mathbf{g}_i \cdot \hat{S}_i + \gamma_e \sum_i \hat{I}_i \cdot \mathbf{A}_i \cdot \hat{S}_i - 2\gamma_e J \hat{S}_1 \cdot \hat{S}_2 + \hat{S}_1 \cdot \mathbf{T} \cdot \hat{S}_2 \qquad (2)$$

where the first term is the Zeeman interaction of each electron spin with magnetic field $\vec{B}_0$, depending on the $\mathbf{g}_i$ tensor; the second term is the hyperfine interaction of each ^{14}N/unpaired electron, defined with respect to the hyperfine tensor $\mathbf{A}_i$; the third and fourth terms are the electron exchange and spin−spin dipolar terms, respectively. Although all hyperfine tensors are

(25) Marshall, G. R.; Hodgkin, E. E.; Langs, D. A.; Smith, G. D.; Zabrocki, J.; Leplawy, M. T. *Proc. Natl. Acad. Sci. U.S.A.* **1990**, *87*, 487.
(26) Smythe, M. L.; Huston, S. E.; Marshall, G. R. *J. Am. Chem. Soc.* **1993**, *115*, 11594.
(27) Fiori, W. R.; Miick, S. M.; Millhauser, G. L. *Biochemistry* **1993**, *32*, 11957.
(28) Zhang, L.; Hermans, J. *J. Am. Chem. Soc.* **1994**, *116*, 11915.
(29) Paterson, Y.; Rumsey, S.; Benedetti, E.; Némethy, G.; Scheraga, H. A. *J. Am. Chem. Soc.* **1981**, *103*, 2947.
(30) Burla, M. C.; Camalli, M.; Carrozzini, B.; Cascarano, G. L.; Giacovazzo, C.; Polidori, G.; Spagna, R. *J. Appl. Crystallogr.* **2003**, *36*, 1103.
(31) Sheldrick, G. M. *SHELXL 97. Program for the Refinement of Crystal Structures*; University of Göttingen: Göttingen, Germany, 1997.
(32) Polimeno, A.; Freed, J. H. *J. Phys. Chem.* **1995**, *99*, 10995.
(33) (a) Meirovitch, E.; Igner, D.; Igner, E.; Moro, G.; Freed, J. H. *J. Chem. Phys.* **1982**, *77*, 3915. (b) Schneider, D. J.; Freed, J. H. *Adv. Chem. Phys.* **1989**, *73*, 487.

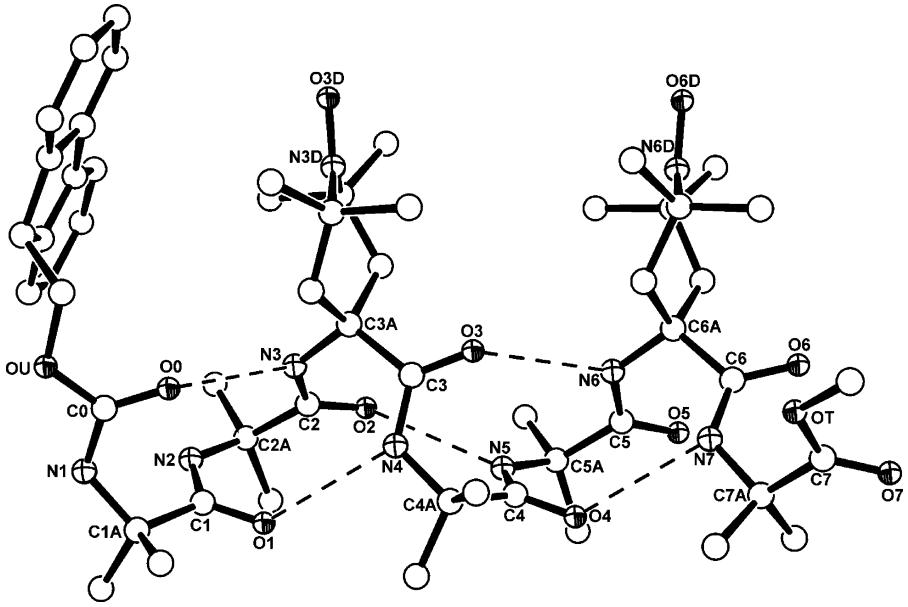

Figure 2. X-ray diffraction structure of heptapeptide **1**. Intramolecular H-bonds are represented by dashed lines.

available from our quantum mechanical (QM) computations, we neglect explicit coupling with nuclei other than ^{14}N since the small inhomogeneous broadening in the spectra resulting from coupling with hydrogen nuclei is essentially temperature and solvent independent. Notice, however, that hydrogen hyperfine tensors could be used to perform a partial averaging of an extended SLE equation leading to explicit evaluation of broadening constants and of their weak temperature dependence.

Several relaxation processes can be invoked and modeled accordingly within the SLE formalism by carefully choosing the time evolution operator $\hat{\Gamma}$. Here, following ref 7, we shall limit our description to the case of a freely (and rigidly) orienting molecule in space, subjected to a simple diffusive motional regime. The ESR spectrum is obtained as the Fourier−Laplace transform of the correlation function for the *x*-components of the magnetizations which is dependent on the nuclear spin.

4. Results and Discussion

The structure of heptapeptide **1**, as determined by single-crystal X-ray diffraction analysis, is illustrated in Figure 2. Relevant geometrical parameters are listed in Table 1. With the peptide being achiral and crystallizing in a centrosymmetric space group, molecules of both handedness are found in the crystals. A molecule of the righ-handed screw sense has been chosen as the asymmetric unit. The peptide backbone is folded into a regular 3_{10}-helix, stabilized by five, consecutive, N−H ... O═C intramolecular hydrogen bonds of the $i + 3 \rightarrow i$ type. The C-terminal Aib(7) residue, external to the H-bonding pattern, adopts a helical conformation with a screw sense opposite to that of the preceding residues. The piperidinyl rings of the two TOAC residues are oriented roughly perpendicular to the helix axis and parallel to each other, the angle between normals to their average planes being 4.5(1)°. The angle between the two N−O bonds is 10.9(4)°.

The piperidinyl rings of both TOAC residues are found in the $^6T_2$ twist conformation (relative to the ring atom sequence $N^{\delta}-C^{\gamma 2}-C^{\beta 2}-C^{\alpha}-C^{\beta 1}-C^{\gamma 1}$, where $C^{\beta 1}$ refers to the *pro-S* C^{β} atom). For a statistical analysis of TOAC ring conformations in the crystal state, see ref 17b. The puckering parameters are the following: $Q_T = 0.595(4)$ Å, $\phi_2 = 92.3(4)°$, $\theta_2 = 86.2(4)°$ for TOAC(3), and $Q_T = 0.634(4)$ Å, $\phi_2 = 88.8(4)°$, $\theta_2 = 90.1(3)°$ for TOAC(6).[34]

The hydroxyl groups of the two cocrystallized TFE molecules are H-bonded to the nitroxide O^{δ} and the carbonyl oxygen atom, respectively, of TOAC(6) within the same asymmetric unit. In the packing mode, peptide molecules are linked head-to-tail through an intermolecular H-bond between the N−H group of Aib(1) and the Aib(7) carbonyl oxygen atom of a $(x, y - 1, z)$ symmetry related molecule, giving rise to rows of molecules along the *b* direction.

The availability of a relatively cheap QM approach able to reproduce the experimental trends would allow us to gain further insight on the interplay of different factors in favoring different helical structures. In view of previous quite encouraging experiences,[35−37] we have thus undertaken a systematic study of heptapetide **1** by a DFT approach. The optimized structures have been obtained by PBE0/6-31G(d) calculations[38] in the gas phase and in aqueous solution, using in the latter case the so-called polarizable continuum model (PCM)[2,39] to represent bulk solvent effects (Figure 3). All energy minima obtained in the gas phase are characterized by a 3_{10}-helical backbone with different conformations (chair or twist) of the nitroxide ring, the absolute minimum corresponding to twist arrangements of both piperidinyl rings. All of the geometrical parameters of the absolute energy minimum issuing from QM computations are in remarkable agreement with those derived from the X-ray diffraction analysis of the same peptide (see Table 1), including local environment of the nitroxide moiety and the hydrogen bond network. This finding is interesting since the preferred conformation of the nitroxide ring depends on the backbone conformation: specifically, twist rings are favored by helical backbones, whereas chair rings are more stable for extended backbones or

(34) Cremer, D.; Pople, J. A. *J. Am. Chem. Soc.* **1975**, *97*, 1354.
(35) Improta, R.; Benzi, C.; Barone, V. *J. Am. Chem. Soc.* **2001**, *123*, 12568.
(36) Improta, R.; Mele, F.; Crescenzi, O.; Benzi, C.; Barone, V. *J. Am. Chem. Soc.* **2002**, *124*, 7857.
(37) Langella, E.; Improta, R.; Barone, V. *J. Am. Chem. Soc.* **2002**, *124*, 11531.
(38) Adamo, C.; Barone, V. *J. Chem. Phys.* **1999**, *110*, 6158.
(39) Cossi, M.; Scalmani, G.; Rega, N.; Barone, V. *J. Chem. Phys.* **2002**, *117*, 43.

Table 1. Comparison between the X-ray Diffraction and Computed Geometrical Parameters for Heptapeptide **1** (Distances in Å and Angles in deg)[a]

				TOAC3			TOAC6		
helix		N...N	O...O	NO	CNC	CNO...C	NO	CNC	CNO...C
3_{10}	gas-phase	6.57	6.80	1.272	123.1	−177.9	1.273	123.0	−178.0
3_{10}	PCM/H_2O	6.51	6.74	1.273	123.0	−179.8	1.274	123.0	−179.2
α	PCM/H_2O	7.97	9.27	1.273	122.6	−179.1	1.273	122.5	−179.7
3_{10}	X-ray	6.40	6.59	1.276	124.8	−178.6	1.279	123.7	−177.6

	ϕ angle				ψ angle			
	3_{10}	3_{10}	α	3_{10}	3_{10}	3_{10}	α	3_{10}
	gas-phase	PCM/H_2O	PCM/H_2O	X-ray	gas-phase	PCM/H_2O	PCM/H_2O	X-ray
1	−59.2	−56.8	−58.6	−57.2	−29.9	−32.4	−29.9	−40.3
2	−54.1	−53.9	−50.9	−54.6	−24.3	−24.8	−32.3	−33.1
3	−52.4	−51.7	−50.2	−57.6	−33.7	−34.2	−46.8	−24.3
4	−55.1	−53.8	−61.0	−51.5	−28.1	−29.5	−47.1	−28.3
5	−58.2	−55.5	−64.5	−50.5	−20.1	−25.8	−46.2	−32.0
6	−59.1	−58.9	−64.3	−55.3	−31.1	−31.6	−41.0	−39.0

	$NC^{\alpha}C'$ angle				$C^{\beta 2}C^{\alpha}C^{\beta 1}$ angle			
	3_{10}	3_{10}	α	3_{10}	3_{10}	3_{10}	α	3_{10}
	gas-phase	PCM/H_2O	PCM/H_2O	X-ray	gas-phase	PCM/H_2O	PCM/H_2O	X-ray
1	110.9	110.5	110.7	110.0	110.6	110.5	110.5	110.3
2	111.7	111.2	110.4	111.2	110.5	110.4	110.2	112.4
3	109.2	109.1	108.5	109.8	110.9	110.8	110.6	111.2
4	112.0	114.4	109.9	110.5	110.4	110.2	109.6	111.8
5	112.7	111.9	110.2	111.6	110.1	110.0	109.4	110.9
6	110.0	110.0	108.9	108.7	110.7	110.5	110.2	110.4

helix		HB1	HB2	HB3	HB4	HB5
3_{10}	gas-phase	2.02	2.11	2.05	2.12	2.06
3_{10}	PCM/H_2O	1.96	2.02	2.02	2.04	1.99
α	PCM/H_2O	1.97	2.13	2.18	2.19	-
3_{10}	X-ray	2.22	2.14	2.22	2.18	2.17

[a] Estimated standard deviations for the crystallographically derived parameters are in the ranges 0.004−0.007 Å, 0.3°−0.5°, and 0.3°−0.6° for bond distances, bond angles, and torsion angles, respectively.

around turns.[17b,40] Furthermore, a good match of the intermolecular distance between nitroxide groups is mandatory for the computation of reliable long-range *J* and spin−spin dipolar interactions. Starting from the structure optimized in the gas phase, two different energy minima are obtained in aqueous solution, corresponding to 3_{10}- and α-helical arrangements of the backbone (Figure 3). While the 3_{10}-helix is significantly more stable (by 2.1 kcal/mol), it is well-known that current density functionals overstabilize the 3_{10}-helix with respect to the α-helix due to the lack of dispersion interactions. We have thus added these terms by the procedure and parameters recently optimized and validated by Grimme[41] and coded in the Gaussian package by one of us. It is remarkable that the α-helix now corresponds to the absolute energy minimum (more stable than the 3_{10}-helix by 3.0 kcal/mol) in aqueous solution, so that a transition between different helical forms is expected as a function of solvent polarity. The 3_{10}-helix differs in its intramolecular hydrogen-bonding pattern from the α-helix: the C═O ... H−N hydrogen bonds are seen between residues *i* and *i* + 3 in the former and between residues *i* and *i* + 4 in the latter helix. Differences in the backbone dihedrals ϕ and ψ are less than 15° for the two helical conformations. The 3_{10}-helix has one additional intramolecular hydrogen bond with respect to the α-helix (Table 1). Upon increasing the solvent dielectric constant, the effective strength of the extra hydrogen bond is reduced, and the closer nonbonded contacts in the 3_{10}-helix may disfavor this conformation. In polar environments, the α-helix is stabilized by its more favorable solute−solvent electrostatic interactions and intramolecular steric interactions. Lower polarity solvents are associated with an increased relative stability of the 3_{10}-helix that it is largely due to the additional intrahelical hydrogen bond characterizing this conformation. Although experimental evidence for such trends has been reported in previous works[15,16] and will be confirmed in the following by simulation of ESR spectra, it is remarkable that *a priori* QM computations lead to the same conclusion.

In the 3_{10}-helix the distance (*d*) between the nitroxide oxygen atoms of the two TOAC residues at relative positions *i*, *i*+3 is about 6.5 Å, while in the α-helix this distance is significantly longer (8.0 Å). In general, the 3_{10}-helix exhibits $d(i, i + 3) < d(i, i + 4)$, whereas in the α-helix the opposite holds true. The experimentally observed peptide helices are somewhat distorted from their ideal geometries,[18,19] but the difference in the relative side-chain distances between the 3_{10}- and α-helices persists.

The above 3D-structures have been next used to compute the magnetic tensors in different solvents, including in the case of chloroform and methanol the solvent molecules forming hydrogen bonds with the nitroxide group. Typical optimized structures are shown in Figure 4.

Let us recall that the orbitals determining the magnetic properties of nonconjugated nitroxides are strongly localized onto the NO moiety (Figure 5), so that the principal axes of

(40) D'Amore, M.; Improta, R.; Barone, V. *J. Phys. Chem. A* **2003**, *107*, 6264.
(41) Grimme, S. *J. Comput. Chem.* **2004**, *25*, 1463.

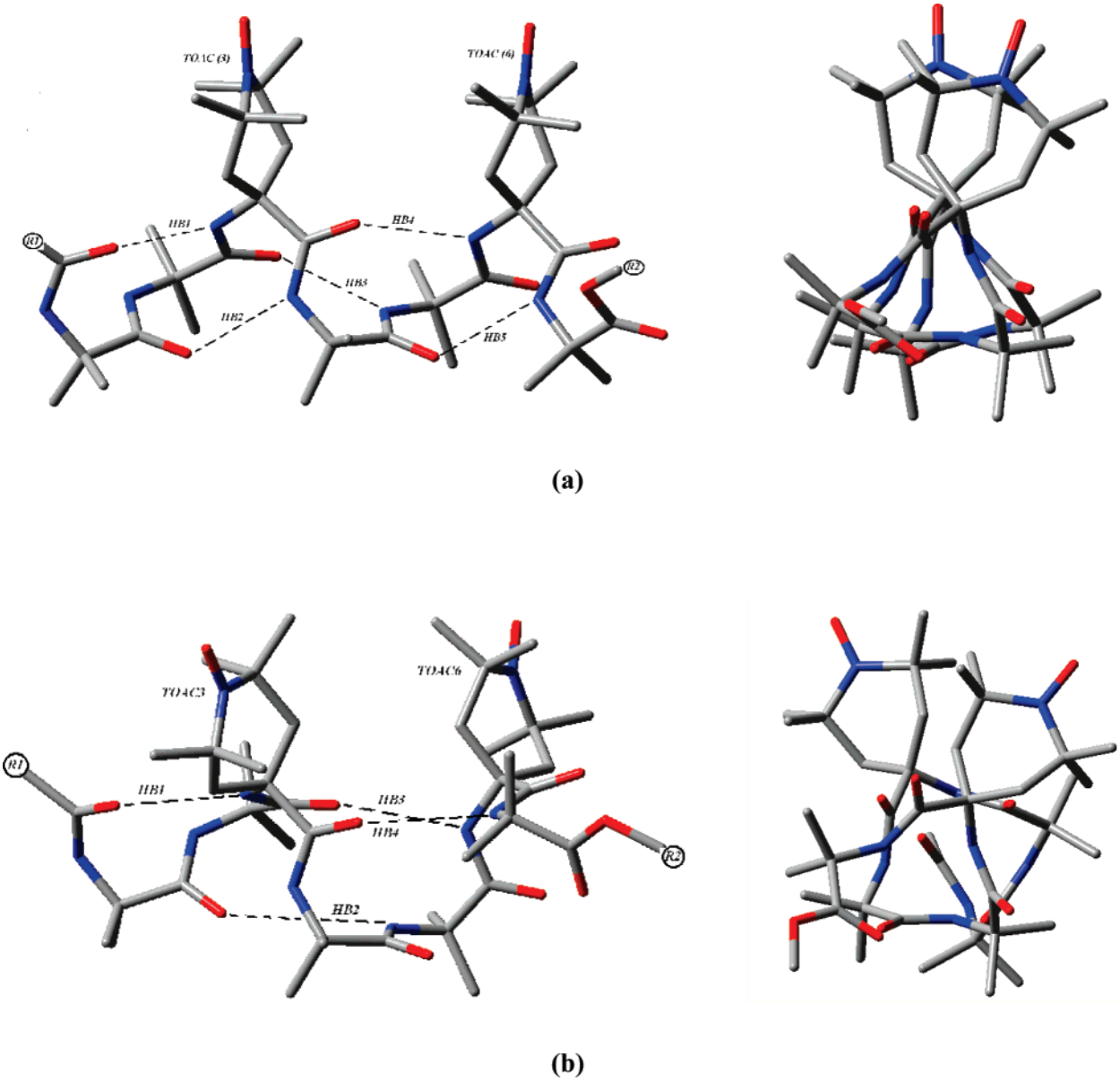

Figure 3. Optimized structure of heptapeptide **1**: View along (right) and orthogonal (left) the helix axis of the (a) 3_{10}-helix and (b) α-helix secondary structure.

both hyperfine and **g** tensors are well aligned along the NO bond (by convention the *x*-axis) and with the average direction of π-orbitals (*z*-axis).

The **g** tensors computed by last generation density functionals are usually in good agreement with the experiments[42] and have been used without further corrections in the simulation of ESR spectra. Table 2 shows the values of the principal axes components reported in ppm units relative to the free electron value in order to highlight the difference between the values in different solvents. The most important contribution to **g** shifts comes from an electronic excitation from the SOMO−1 (an in-plane lone pair, hereafter referred to as *n*) to the SOMO (an out-of-plane π^* orbital), both of which are sketched in Figure 5. The dependence of the **g** tensor on solvent polarity is related to the selective stabilization of lone pair orbitals by polar solvents: this increases the $n \rightarrow \pi^*$ gap with the consequent reduction of **g** tensor shifts (especially g_{xx}). Together with this purely electrostatic contribution, formation of solute−solvent H-bonds also concurs to the stabilization of lone pair orbitals and, once again, to a decrease of **g** tensor shifts. In any case, structural and solvent effects on **g** are well within experimental uncertainty: thus, constant values of 2.009, 2.006, and 2.003 have been used in the fitting of all spectra for the principal axes of the **g** tensor.

The situation is more complex for nitrogen hyperfine tensors **A**, which can be decomposed into two terms: the isotropic hyperfine term (a_{iso}) and dipolar contributions (**B**). The results reported in Table 3 show that the **B** tensor has the same behavior as the **g** tensor and that, to a good approximation, its principal axes are parallel (B_{zz}) or perpendicular (B_{xx}, B_{yy}) to the NO π orbital with $B_{xx} \approx B_{yy}$. It is well-known that accurate estimates of isotropic hyperfine couplings for nitroxides can be obtained only using very demanding theory levels, like, e.g., quadratic configuration interaction including single and double excitations

(42) (a) Ciofini, I.; Barone, V.; Adamo, C. *J. Chem. Phys.* **2004**, *121*, 6710. (b) Barone, V.; Carbonniere, P.; Pouchan, C. *J. Chem. Phys.* **2005**, *122*, 224308.

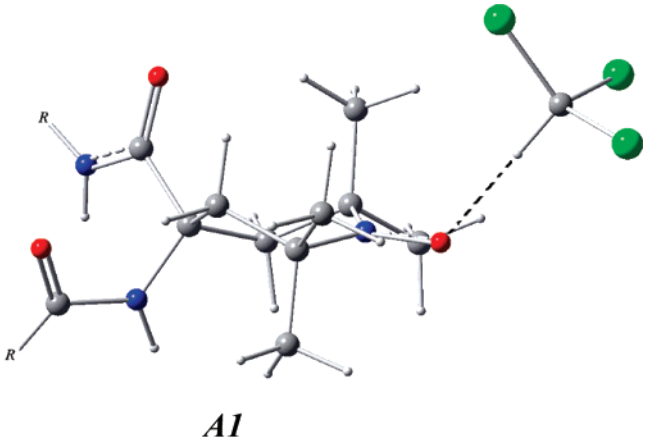

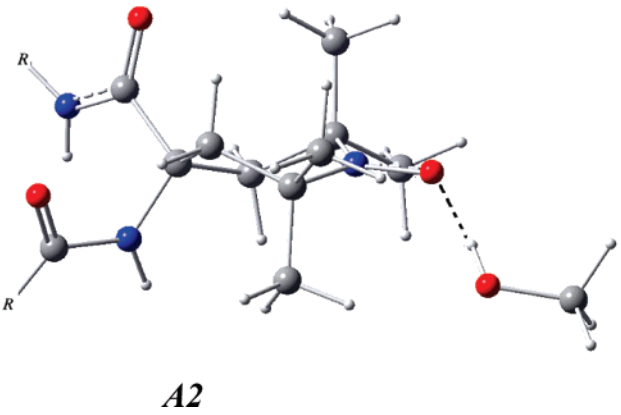

Figure 4. Structures of the TOAC-solvent complexes: twist conformation with $CHCl_3$ (***A1***); twist conformation with methanol (***A2***). R = peptide chain.

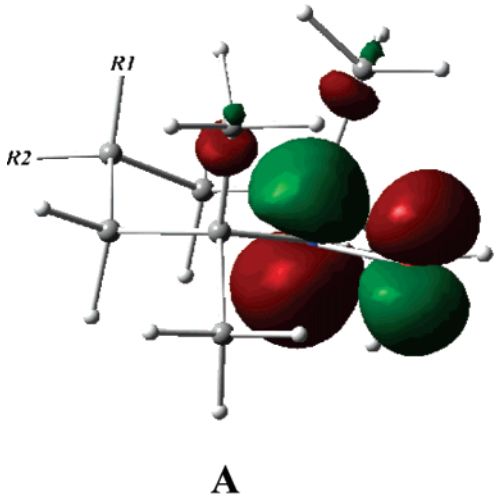

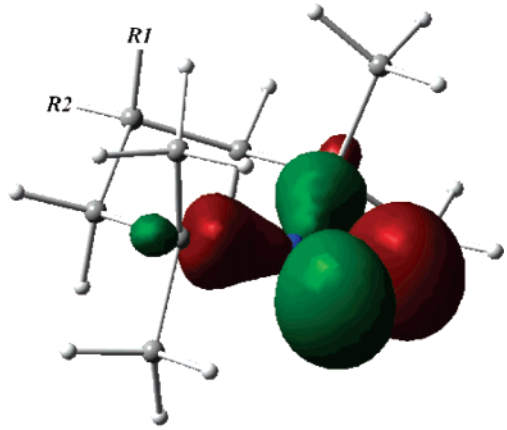

Figure 5. Sketch of SOMO (A) and SOMO−1 (B) of TOAC (R1 = −COOH, R2 = −NH2) in two different orientations.

Table 2. Gyromagnetic Tensors (ppm) Computed in Different Solvents[a]

	δg_{xx}	δg_{yy}	δg_{zz}
gas-phase	6829	3787	−262
toluene ($\epsilon = 2.3$)	6674	3754	−262
chloroform ($\epsilon = 4.9$)	6579 (6349)	3733 (3598)	−262 (−232)
methanol ($\epsilon = 32$)	6472 (5912)	3709 (3580)	−262 (−253)
acetonitrile ($\epsilon = 36$)	6470	3709	−262

[a] Values in parentheses are obtained including one specific solvent molecule for each NO moiety (see Figure 4).

(QCISD) with purposely tailored basis sets, possibly integrated into an ONIOM-like approach.[40] We have, however, recently developed a new basis set (N06) that, coupled to the PBE0 functional, promises to overcome this problem. Indeed, the computed a_{iso} for the closely related TEMPO (2,2,6,6-tetramethylpiperidine-*N*-oxyl) radical in cyclohexane (15.23) and in toluene (15.32) are in remarkable agreement with the experimental values (15.28 and 15.40 G, respectively).[43,44] The computed values for the chair conformation of TOAC are very close, whereas significantly lower values (12.38 and 12.54 G) are obtained for the twist structure. This is related to the different pyramidality around nitrogen: in particular, the nearly planar arrangement characterizing the twist structure leads to the lack of any contribution of nitrogen *s* orbitals to the orbital formally containing the unpaired electron with the consequent strong reduction of a_{iso}. However, vibrational averaging effects, which are essentially negligible for chair structures, become quite significant for the nearly planar nitroxide moieties characterizing twist structures. Without entering into a detailed description of the effective one-dimensional model we have used to estimate these effects,[45,46] we just mention that a nearly constant vibrational correction of 1.7 G is obtained for all twist structures. It is noteworthy that, after this correction, twist and chair conformations have comparable hyperfine couplings, which show, furthermore, a distinct solvent dependence (see Table 4). In particular, solvent polarity and formation of solute−solvent hydrogen bonds concur to the selective stabilization of the nitroxide resonance structure involving at the same time formal charge separation and increased spin density on nitrogen.[45] The final values computed for the different solvents are as follows: 14.3 (toluene), 14.8 (acetonitrile), 15.0 (chloroform), and 15.3

(43) Lucarini, M.; Pedulli, G. F. *Chem. Phys. Phys. Chem.* **2002**, *3*, 789.
(44) Aurich, H. G.; Hahn, K.; Stork, K.; Weiss, W. *Tetrahedron*, **1977**, *33*, 369.
(45) Improta, R.; Barone, V. *Chem. Rev.* **2004**, *104*, 1231.
(46) (a) Barone, V. *J. Phys. Chem.* **1995**, *99*, 11659. (b) Barone, V.; Subra, R. *J. Chem. Phys.* **1996**, *104*, 2630. (c) Barone, V. *Chem. Phys. Lett.* **1996**, *262*, 201.

Table 3. Dipolar Hyperfine Tensors (in Gauss) Computed for Heptapeptide **1** in Different Solvents[a]

	B_{xx}	B_{yy}	B_{zz}
gas-phase	−8.70	−8.46	17.16
toluene (ϵ=2.3)	−8.92	−8.70	17.62
chloroform (ϵ=4.9)	−9.05 (−9.38)	−8.85 (−9.24)	17.90 (18.62)
methanol (ϵ=32)	−9.19 (−9.59)	−9.01 (−9.48)	18.20 (19.06)
acetonitrile (ϵ=36)	−9.19	−9.02	18.21

[a] Values in parentheses are obtained including one specific solvent molecule for each nitroxide moiety (see Figure 4).

Table 4. Calculated Nitrogen Isotropic Hyperfine Couplings (in Gauss) for the Optimized 3_{10}-Helix of Heptapeptide **1** Are Compared with Fitted Values (Best Fit)[a]

	$a°_{iso}$	Δvib	Δ_{1S}	best calcd	best fit
gas-phase	12.2	1.7			
toluene	12.6	1.7	-	14.3	14.5
chloroform	12.8	1.7	0.58	15.1	15.0
methanol	13.1	1.7	0.61	15.4	15.3
acetonitrile	13.1	1.7	-	14.8	14.8

[a] The final calculated values (best calcd) include electronic values at the energy minimum ($a°_{iso}$), vibrational averaging (Δ_{vib}), and, for protic solvents, the contribution of a single explicit solvent molecule (Δ_{1S}). The last column reports the optimized values of the isotropic hyperfine coupling.

G (methanol), where 1 G = 10^{-4} T. To fine-tune the simulated spectra we set $A_{XX} \approx A_{YY} = A_{\perp}$ and $A_{ZZ} = A_{||}$ and then fit the isotropic value $a_{iso} = (2A_{\perp} + A_{||})$ by keeping constant the anisotropy ratio $R = A_{\perp}/A_{||} = 0.13$.

Hyperfine and gyromagnetic tensors have a local character and are thus only marginally influenced by the long-range interactions modified by conformational changes (e.g., transition from the 3_{10}- to the α-helix). The other magnetic terms (J and spin−spin dipolar interaction) have a long-range character and can provide, in principle, a signature for the different helical structures. The J terms have been calculated from differences between triplet and singlet energies by the so-called broken-symmetry approach.[47] Although the computed J values are slightly different for the 3_{10}- and the α-helix (140.8 and 139.5 G, respectively, at the PBE0/N06 level), this trend does not allow us to gain further structural information, since (as we shall see) all values larger than 130 G are compatible with experimental data.

Usually, the spin−spin dipolar term is calculated by assuming that the two unpaired electrons are localized at the center of the N− O bonds of the two TOAC residues. Then, the two electrons are considered just as two point magnetic dipoles and the interaction term depends on the distance between the two localized electrons:

$$\mathbf{T} = \frac{\mu_0}{4\pi}\frac{g_e^{2}\beta_e^{2}}{\hbar r^3}\left[\mathbf{1}_3 - \frac{3}{r^2}\begin{pmatrix} r_x^2 & r_x r_y & r_x r_z \\ r_x r_y & r_y^2 & r_y r_z \\ r_x r_z & r_y r_z & r_z^2 \end{pmatrix}\right]$$

Obviously, this is just a rough approximation which could break down at not too long distances. On the other hand, a complete QM computation is hardly feasible for the large systems we are interested in. Thus, the strong localization of the magnetic orbitals of nonconjugated nitroxides (see Figure 5) suggests that, for not too short distances between NO moieties, a reliable approximation would be to fit the SOMO electron density by linear combinations (with equal weights) of effective nitrogen and oxygen valence Slater orbitals. Then, the tensorial operator $\hat{\mathbf{T}}$ has components

$$\hat{T}_{\alpha,\beta} = \frac{r_{12}^{2}\delta_{\alpha,\beta} - 3(\mathbf{r}_{12})_{\alpha}(\mathbf{r}_{12})_{\beta}}{r_{12}^{5}}$$

where $r_{12} = |\mathbf{r}_{12}| = |\mathbf{r}_1 - \mathbf{r}_2|$ is the vector between the two electrons, $\alpha,\beta = X,Y,Z$, and $(\mathbf{r}_{12})_{\alpha}$ is the component along α of vector $\mathbf{r}_{12}$. In the present case, only the $T^{(2,0)}$ component (proportional to T_{zz} in Cartesian coordinates) contributes significantly to the dipolar tensor. Figure 6 shows the trend of $|T^{(2,0)}|$ *versus* the distance between the two TOAC nitroxides and highlights the position of the 3_{10}-helix and the α-helix with respect to the distance between the TOAC residues. The difference between the point-dipole approximation and the quantum mechanical values of the dipolar tensor is higher in the 3_{10}-helix structure, in which the distance between the two nitroxides is lower if compared to that of the α-helix.

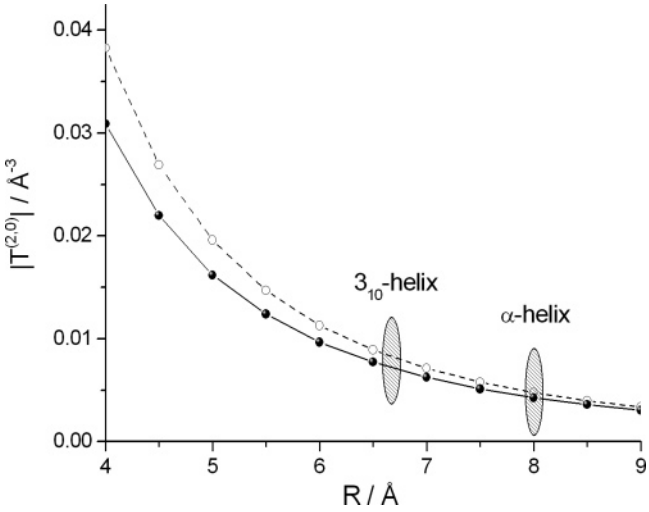

Figure 6. Trend of $|T^{(2,0)}|$ *versus* distance calculated with the point dipole (dashed line) and localized quantum mechanical (solid line) approaches.

The rotational dynamics is controlled by the rotational diffusion tensor **D**, which, in turn, can be evaluated from the molecular shape and macroscopic solvent properties.[7] In particular, evaluation of the diffusion properties of **1** is based on a hydrodynamic approach.[5,6] The molecule is seen as an ensemble of N segments, each constituted by a sphere representing atoms or groups of atoms and immersed in a homogeneous isotropic fluid of known viscosity. First, we calculate a form of the friction tensor for the nonconstrained extended atoms ξ and one for the constrained atoms Ξ. The simplest model for interacting spheres in a fluid has been used, in which the translational friction $\xi(T)$ of a sphere at a specific temperature is given by the Stokes law $\xi(T) = CR\eta(T)\pi$ dependent on the viscosity $\eta(T)$ of the solvent and on the hydrodynamic boundary conditions. The diffusion tensor (partitioned in translational, rotational, internal, and mixed blocks) can be obtained as the inverse of the friction tensor.[48] We can write the rotational diffusional tensor (already diagonalized in the molecular frame) in the form $\mathbf{D}(T) = D(T)\mathbf{d}$,

(47) Improta, R.; Kudin, K. N.; Scuseria, G. E.; Barone, V. *J. Am. Chem. Soc.* **2002**, *124*, 113.

(48) Yawada, Y.; Tsuneda, T.; Yanagisawa, S.; Yanai, T.; Hirao, K. *J. Chem. Phys.* **2004**, *120*, 8425.

where $D(T) = k_B T/\xi(T)$ is the translational diffusional coefficient of a sphere of radius R at temperature T and **d** is a diagonal tensor depending only on the molecular geometry, with values $d_{xx} = 1.71 \times 10^{16}$, $d_{yy} = 1.83 \times 10^{16}$, and $d_{zz} = 5.75 \times 10^{16}$ m^{-2} for the 3_{10}-helix and $d_{xx} = 1.88 \times 10^{16}$, $d_{yy} = 2.01 \times 10^{16}$, and $d_{zz} = 4.91 \times 10^{16}$ m^{-2} for the α-helix. The same procedure, previously employed[7] for the calculation of the diffusion tensor at different temperatures, and based on available viscosity data for the solvents considered,[49] was used to calculate the temperature- and solvent-dependent rotational diffusion tensors. The larger difference between the value of the diffusion tensor for the 3_{10}-helix and the α-helix is computed for the ratio of the z component (d_{ZZ}) and the x component (d_{XX}) of the tensor. For all the temperatures and solvents investigated, this ratio is 3.36 for the 3_{10}-helix and 2.61 for the α-helix. These different values can be explained by simply considering the shape of the two secondary structures illustrated in Figure 3. A higher value of the ratio is related to a long and slim shape of the molecule (Figure 3b) while a lower value indicates that the molecule is shorter and wider (Figure 3a).

Simulated spectra in different solvents exhibit different sensitivities with respect to the magnetic and diffusion calculated parameters. In particular, simulations, as expected, are not sensitive to changes in the electron exchange interaction J when $J > 130$ G. The dependence on the values of the components of the diffusion tensor **D** is more significant: variations within a 10% range of the proposed values, calculated according to the hydrodynamic approach, cause a significant change in the intensity and widths of the peaks. Moreover, the spectra dependence on the temperature is perfectly reproduced by the calculated **D** tensor. Sensitivity upon the dipolar interaction tensor **T** is also relevant. The spectrum is controlled by the dominant $T^{(2,0)}$ component, which causes noticeable variations when changed within 10%. An overestimation of **T**, corresponding for instance to use of the approximate point dipole formulation, leads to an increase of the width and a decrease of the intensity of all peaks. Finally it is well-known that the general dependence of CW-ESR spectra upon the **g** and **A** tensor component values and orientation Euler angles is highly pronounced and no significant adjustment is possible with respect to the calculated values which are in very good agreement with the experimental observations.

The SLE computations were performed for four different solvents: acetonitrile (MeCN), methanol, toluene, and chloroform. It is worthwhile to remark that the overall computational protocol has been organized in a novel suite of computational codes which present significant advancements with respect to the existing packages for the interpretation of ESR spectra, namely the integration of the QM and stochastic dynamics parts, the extension to multiple radicals and nuclei, and finally the increased computational efficiency based on a partial on-the-fly evaluation of matrix elements.

For each solvent we examined different temperatures, and at every step a different value of the diffusion tensor was employed owing to the temperature dependence of the viscosity. A common assumption for all solvents is the presence of a monoradical impurity that might arise from the reduction of one of the nitroxide functions. The estimated amount of the impurity is below 4%, a low but still appreciable percentage. It is noteworthy that the optimized values of a_{iso} (the only adjustable parameters in our protocol) are very close to their QM counterparts for all solvents (see Table 4).

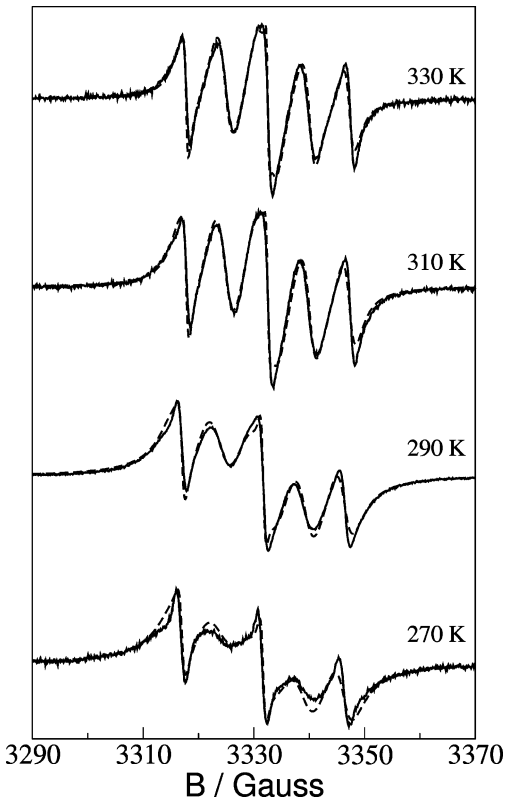

Figure 7. Experimental (solid lines) and theoretical (dashed lines) CW-ESR spectra of heptapeptide **1** in MeCN at temperatures 330, 310, 290, and 270 K.

Figure 7 collects four theoretical spectra for the heptapeptide **1** in MeCN and their experimental counterparts at four different temperatures: 330, 310, 290, and 270 K. From the simulations it appears that in this solvent only the 3_{10}-helix occurs, i.e., $p_\alpha = 0$, $p_{3_{10}} = 98$, $p_{mono} = 2\%$ at all temperatures.

Figure 8 shows five theoretical and experimental spectra in methanol solution in the temperature range 280 to 320 K. The simulations, which consider that in solution only the α-helix is present, closely reproduce the experimental spectra, $p_\alpha = 97$, $p_{3_{10}} = 0$, $p_{mono} = 3\%$ at all temperatures. Figure 9 collects the simulated and the experimental spectra for a toluene solution in the temperature range 270−350 K. At high temperatures (350, 340, 330, 320 K) the experimental spectra are well reproduced using comparable percentages of α-helix and 3_{10}-helix structures, $p_\alpha = 60$, $p_{3_{10}} = 38$, $p_{mono} = 2\%$. At lower temperatures (below 310 K) the experimental spectra are correctly reproduced by progressively increasing the α-helix percentage, with $p_\alpha = 70$, 75, 78, 92, 98% at 310, 300, 290, 280, 270 K (and constant $p_{mono} = 2\%$).

Figure 10 shows the spectra for a chloroform solutions in the range 290 to 250 K. The experimental spectra are reproduced using only an α-helix structure, $p_\alpha = 96$, $p_{3_{10}} = 0$, $p_{mono} = 4\%$ at all temperatures. From the available literature data[17a] we could expect a high 3_{10}-helix percentage in solution induced by the low polarity of the solvent. However, QM computations show that quite stable hydrogen bonds can be formed between chloroform and both nitroxide and carbonyl groups (see, e.g.,

(49) *Handbook of Chemistry and Physics*, 64th ed.; CRC Press: Boca Raton, FL, 1983; p F-39.

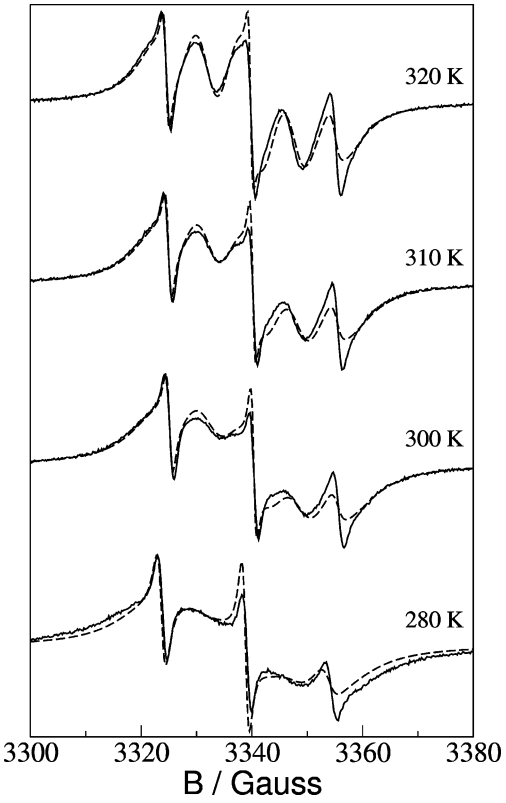

Figure 8. Experimental (solid lines) and theoretical (dashed lines) CW-ESR spectra of heptapeptide **1** in methanol at temperatures 320, 310, 300, and 280 K.

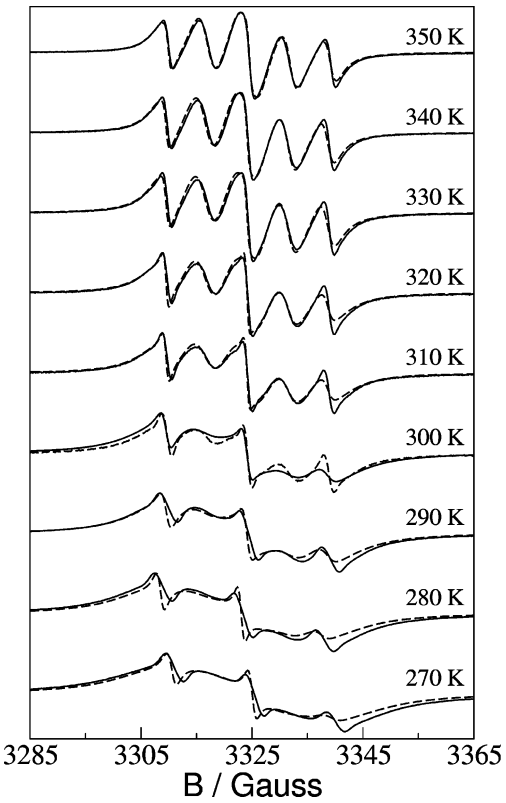

Figure 9. Experimental (solid lines) and theoretical (dashed lines) CW-ESR spectra of heptapeptide **1** in toluene at temperatures 350, 340, 330, 320, 310, 300, 290, 280, and 270 K.

Figure 4), which, in turn, could lead to a switch from the 3_{10}- to the α-helix.[22,23,25]

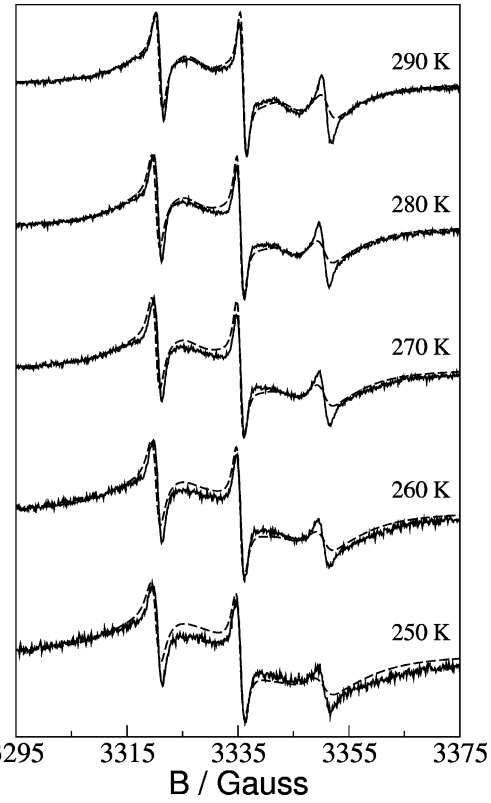

Figure 10. Experimental (solid lines) and theoretical (dashed lines) CW-ESR spectra of heptapeptide **1** in chloroform at the temperatures 290, 280, 270, 260, and 250 K.

Examples of peptides possessing a main-chain length comparable to that of heptapeptide **1**, and largely[50] based upon C^{α}-tetrasubstituted amino acid residues, able to switch from the 3_{10}- to the α-helical conformation upon increasing medium polarity, have been only recently reported.

5. Conclusions

We have reported a detailed analysis of the structural and magnetic properties of a double labeled peptide by an integrated computational and experimental strategy. From a chemical point of view, our results provide evidence on the property of Aib-rich peptides changing their conformation from 3_{10}- to α-helix as a function of increasing polarity and hydrogen-bond donor capability of the solvent: α-helix in protic solvents and at low temperature, whereas 3_{10}-helix in aprotic solvents. The X-ray diffractometric analysis reveals that the peptide assumes a 3_{10}-helical conformation in the crystal state. The 3_{10}-helix is very well reproduced by DFT computations in vacuo and in aqueous solution. Our computational results indicate that in aqueous solution the α-helical conformation becomes the deepest conformational minimum when dispersion interactions are taken into account. Computation of magnetic and diffusion tensors and their feeding in a general computational protocol based on the stochastic Liouville equation allowed us to reproduce in a remarkable way the ESR spectra in different solvents and at different temperatures without any adjustable parameter except the relative percentage of 3_{10}- and α-helices. The favorable scaling of our computational protocol with the dimensions of

(50) Bellanda. M.; Mammi, S.; Geremia, S.; Demitri, N.; Randaccio, L.; Broxterman, Q. B.; Kaptein, B.; Pengo, P.; Pasquato, L.; Scrimin, P. *Chem.—Eur. J.* **2007**, *13*, 407.

the system and its remarkable performances for both structural and magnetic properties might pave the route for systematic studies of spin labeled peptides and proteins.

Acknowledgment. This work was supported by the Ministry for University and Research of Italy (Projects FIRB and PRIN ex-40%) and the National Interuniversitary consortium for Materials Science and Technology (Project PRISMA 2005). All the computations have been performed on the large scale facilities of the VILLAGE network (http://village.unina.it).

Supporting Information Available: X-ray data of heptapeptide. This material is available free of charge via the Internet at http://pubs.acs.org.

JA073516S